Oceanologia (2018) 60, 1—15

Available online at www.sciencedirect.com

ScienceDirect

journal homepage: www.journals.elsevier.com/oceanologia/

ORIGINAL RESEARCH ARTICLE

Total suspended particulate matter in the Porsanger fjord (Norway) in the summers of 2014 and 2015

Jagoda Białogrodzka [a,b,*], Małgorzata Stramska [a,b], Dariusz Ficek [c], Marzena Wereszka [a]

[a] *Department of Earth Sciences, Szczecin University, Szczecin, Poland*
[b] *Institute of Oceanology, Polish Academy of Sciences, Sopot, Poland*
[c] *Department of Environmental Physics, Pomeranian University in Słupsk, Słupsk, Poland*

Received 29 December 2016; accepted 19 June 2017
Available online 6 July 2017

KEYWORDS
Arctic;
Porsanger fjord;
Suspended matter;
Optical measurements

Summary High-latitude fjords, very vulnerable to global change, are impacted by their land and ocean boundaries, and they may be influenced by terrestrial water discharges and oceanic water inputs into them. This may be reflected by temporal and spatial patterns in concentrations of biogeochemically important constituents. This paper analyses information relating to the total suspended matter (TSM) concentration in the Porsanger fjord (Porsangerfjorden), which is situated in the coastal waters of the Barents Sea. Water samples and a set of physical data (water temperature, salinity, inherent optical properties) were obtained during two field expeditions in the spring and summer of 2014 and 2015. Bio-optical relationships were derived from these measurements, enabling optical data to be interpreted in terms of TSM concentrations. The results revealed significant temporal variability of TSM concentration, which was strongly influenced by precipitation, terrestrial water discharge and tidal phase. Spatial distribution of TSM concentration was related to the bathymetry of the fjord, dividing this basin into three subregions. TSM concentrations ranged from 0.72 to 0.132 g m^{-3} at the surface (0—2 m) and from 0.5 to 0.67 g m^{-3} at 40 m depth. The average mineral fraction was estimated to be 44% at surface and 53% at 40 m.

* Corresponding author at: Department of Earth Sciences, Szczecin University, Mickiewicza 16, Szczecin 70-383, Poland. Tel.: +48 58 73 11 600; fax: +48 58 55 12 130.
E-mail addresses: jbialogrodzka@iopan.gda.pl, jagoda.bialogrodzka@gmail.com (J. Białogrodzka).
Peer review under the responsibility of Institute of Oceanology of the Polish Academy of Sciences.

Production and hosting by Elsevier

http://dx.doi.org/10.1016/j.oceano.2017.06.002

1. Introduction

Important oceanic processes, such as the export of carbon and other biogeochemically important material are closely associated with the spatial and temporal variability of suspended particulate matter. The quantity and quality of suspended matter in the water column govern light transfer in surface waters and its availability to primary production, strongly influencing the euphotic depth (Kirk, 2011; Mobley, 1994). In extreme situations, the within-day variability of total suspended matter (TSM) in coastal waters may encompass several orders of magnitude due to the combined effects of physical (*e.g.*, terrestrial water runoff, tidal mixing, aerial deposition of dust) and biological processes (*e.g.*, biological production, aggregation, Montes-Hugo et al., 2012). The high-latitude fjords are among the regions where TSM dynamics is still poorly understood. This is because of the relatively large number of fjords, in which conditions can differ significantly. Traditional shipboard surveys have been sporadic and so far supplied very limited biogeochemical data sets in only a few fjords. In addition, because regional coastal algorithms are non-existent, a quantitative interpretation of the ocean colour data provided by satellite sensors in such locations is not possible.

In general, delivery of suspended matter to Arctic fjords involves four major processes (Syvitski, 1989; Winters and Syvitski, 1992): (1) ice-contact processes associated with tidewater glaciers, (2) rafting by icebergs and sea ice, (3) fluvial discharge of sediment and (4) exchanges of water masses, for example, as a result of oceanic inflows. To extend knowledge of TSM concentrations in high-latitude fjords, *in situ* experiments were carried out in the Porsanger fjord (Porsangerfjorden), one of the largest fjords in northern Norway (Fig. 1). There are no glaciers around the Porsanger fjord, so one would expect TSM concentrations in this fjord to be lower than, for example, in some Greenland and Spitsbergen fjords, where glaciers are present. Nevertheless, it is important to collect information in all types of fjords in order to understand more about how TSM concentrations (both organic and mineral fractions) vary across different time and spatial scales in the Arctic and to enable future extrapolation of this knowledge to large-scale and global estimates.

This paper describes the preliminary results of experiments carried out in the Porsanger fjord. The primary objective was to develop and validate local bio-optical relationships for estimating TSM concentrations from *in situ* optical data and to describe the spatial and temporal variability of TSM concentrations in the Porsanger fjord based on water samples and optical surveys. Traditionally, laboratory biogeochemical analyses of discrete water samples collected at sea have been used to determine the concentrations of suspended material in seawater. However, such analyses are time-consuming and difficult to apply on a large scale. More recently, optical instruments have become popular tools for ocean monitoring (Zaneveld et al., 1994). Unlike classic laboratory analyses of discrete water samples, *in situ* optical measurements provide information about the marine environment at larger spatial and temporal scales. This was the approach taken in the present research.

2. Study region

There are a great many fjords along the Norwegian coast with large variations in topography and dynamics. This paper focuses on the Porsanger fjord, which is located in the in the vicinity of the Barents Sea (Fig. 1) (*ca* 70.0–71.0°N, 25.0–26.5°E). Approximately 100 km long and 15–23 km wide, it has a maximum depth of more than 230 m and extends south-westwards from the northern tip of Norway (North Cape – Nordkapp). It is surrounded by mountains (Fig. 2) that rise to altitudes of more than one thousand metres (Mt. Cahkarassa, 1139 m) on the south-western side

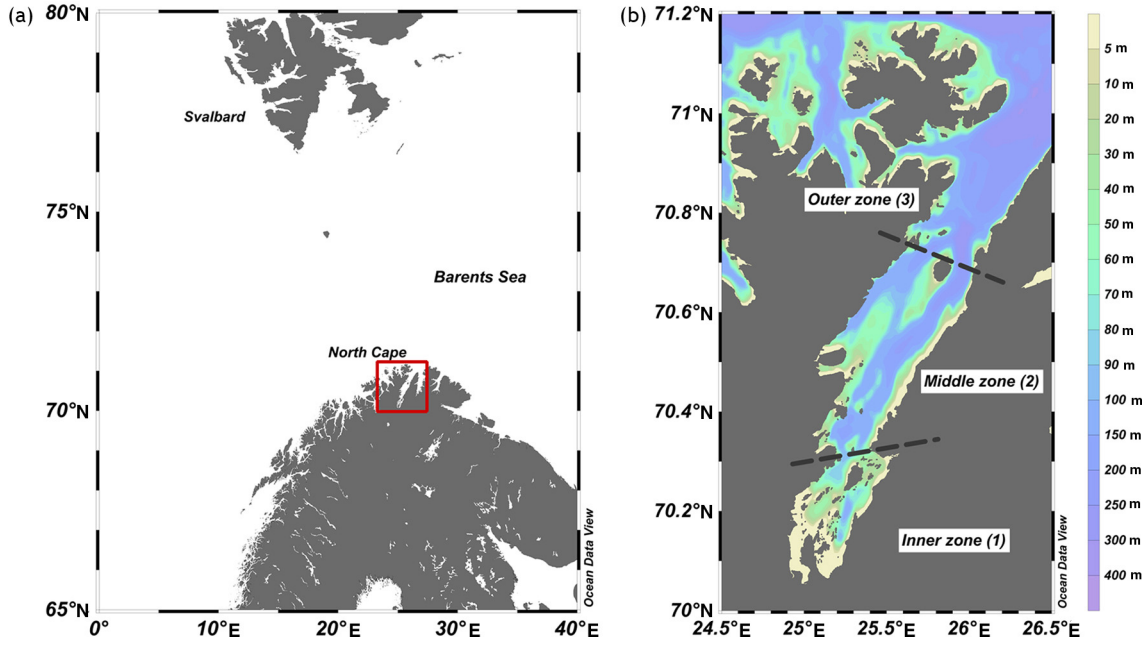

Figure 1 Geographical location of the Porsanger fjord (left panel, red rectangle); fjord bathymetry showing the three subregions investigated (right panel).

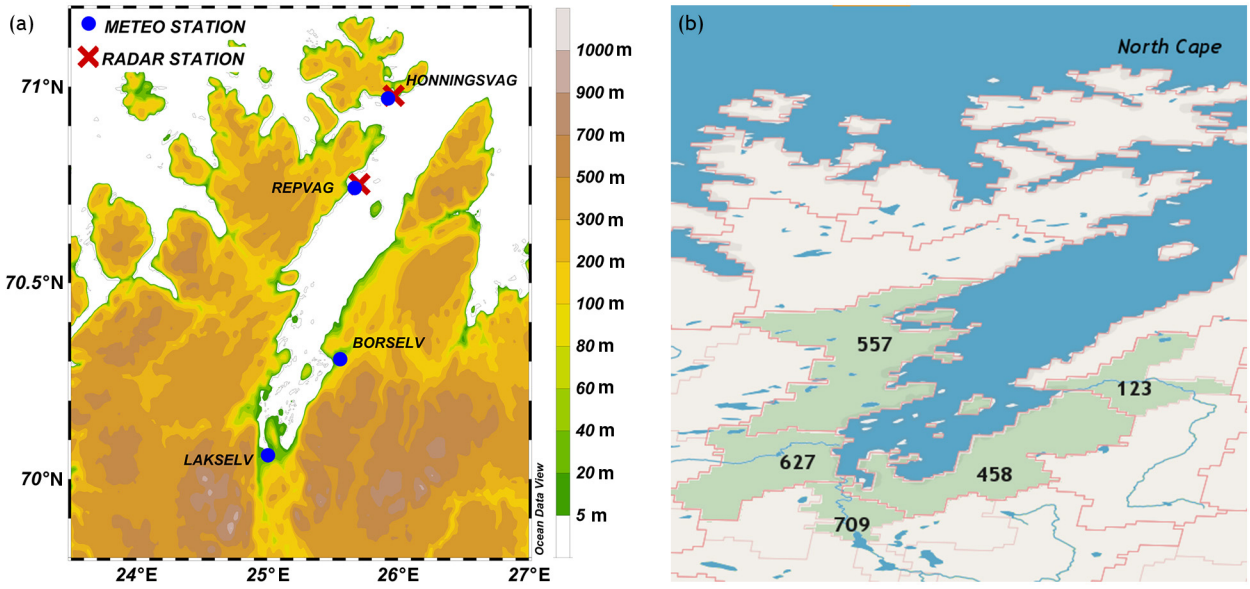

Figure 2 (a) Topography of the land surrounding the Porsanger fjord showing the location of the meteorological and radar stations; (b) E-Hype sub-basins used for water discharge estimates (based on map provided by SMHI HypeWeb).

of the fjord. The land around the fjord, part of the Finnmarksvidda plateau, is mostly about 400 m above sea level.

The land cover varies. Moreover, the region is sparsely populated: only two communities — Honningsvåg and Lakselv — have more than 2000 inhabitants. Farming areas are rather small and are situated mostly around the inner part of the fjord. On the south-eastern, north-western, and north-eastern sides of the fjord there are mostly rocks and tundra vegetation. There is woodland on either side of the middle part of the fjord, but tree growth is stunted as a result of low temperatures and short growing seasons. There are peat bogs all around the fjord.

According to Cushman-Roisin et al. (1994), the width of the Porsanger fjord is approximately three times the deformation radius, so it can be classified as a broad fjord. These same authors reported that the combination of vertical stratification and fjord width can lead, under typical wind stresses, to the development of upwelling on one side of the fjord and downwelling on the other. In line with the classification proposed by Svendsen (1995), Porsanger can be described as a fjord with relatively little water runoff in comparison to other Norwegian fjords, except for the spring and summer seasons, when freshwater runoff significantly influences its hydrography.

With regard to its bathymetry, the Porsanger fjord can be divided into three zones (Fig. 1): an inner zone (subregion 1, extending 0—30 km from the head), a middle zone (subregion 2, located 30—70 km from the head) and an outer zone (subregion 3, 70—100 km from the head). The inner zone is separated from the remainder of the fjord by a 60 m deep sill, situated approximately 30 km from the fjord head: this significantly inhibits water exchange between the inner and outer parts of the fjord. The inner zone environment is very different from the rest of the fjord and supports a unique Arctic ecosystem (Eilertsen and Frantzen, 2007). Beyond the internal sill is the middle part of the fjord: this is separated from the outer zone by the island of Tamsøya, which lies about 70 km from the head of the fjord. Finally, the outer zone ends in a deep sill (180 m); this does not constrain the movements of waters between the fjord and the coastal region of the Barents Sea. Historical observations show evidence of two prevailing wind directions—southerly and northerly—along the fjord's axis. The Porsanger fjord is stratified from May to October as a result of seasonal river runoff and surface warming (Svendsen, 1995). The sea level variability due to tides is significant (about 3 m). The most important tidal component in the surface currents is the semidiurnal one (M2), but winds also have a strong impact on surface currents (Stramska et al., 2016).

3. Methods

Data were collected from June 06 to 29, 2014 and from May 29 to June 18, 2015 during two field expeditions in the Porsanger fjord. Fig. 3a and b shows the sampling stations in 2014 and 2015. At some stations, discrete water samples were collected for TSM determinations, usually near the surface, but also from one or two depths (most often 5 m and 40 or 50 m). The number of water levels sampled at each station depended on the weather conditions, as only a small boat was available for the fieldwork. When the sea was too rough, it was only possible to collect water samples from the surface. In addition to water samples, vertical profiles of inherent optical properties (IOPs) were measured with ac-9 and/or ac-s instruments (WETLabs). More stations were done with the ac-9 in 2014 — this was before a new ac-s instrument was purchased. At some stations data were collected with both instruments, so the different data sets could be compared. The depth range for the profiles was usually 0—50 m, since it was difficult to deploy the instrument packages from that small boat. However, the mixed layer depth varied between 10 and 30 m, so it was usually possible to collect water samples representing both the surface and the deeper water masses. More stations were covered in 2015 than in 2014 (Fig. 3), following some modifications made to the boat to facilitate the deployment of equipment.

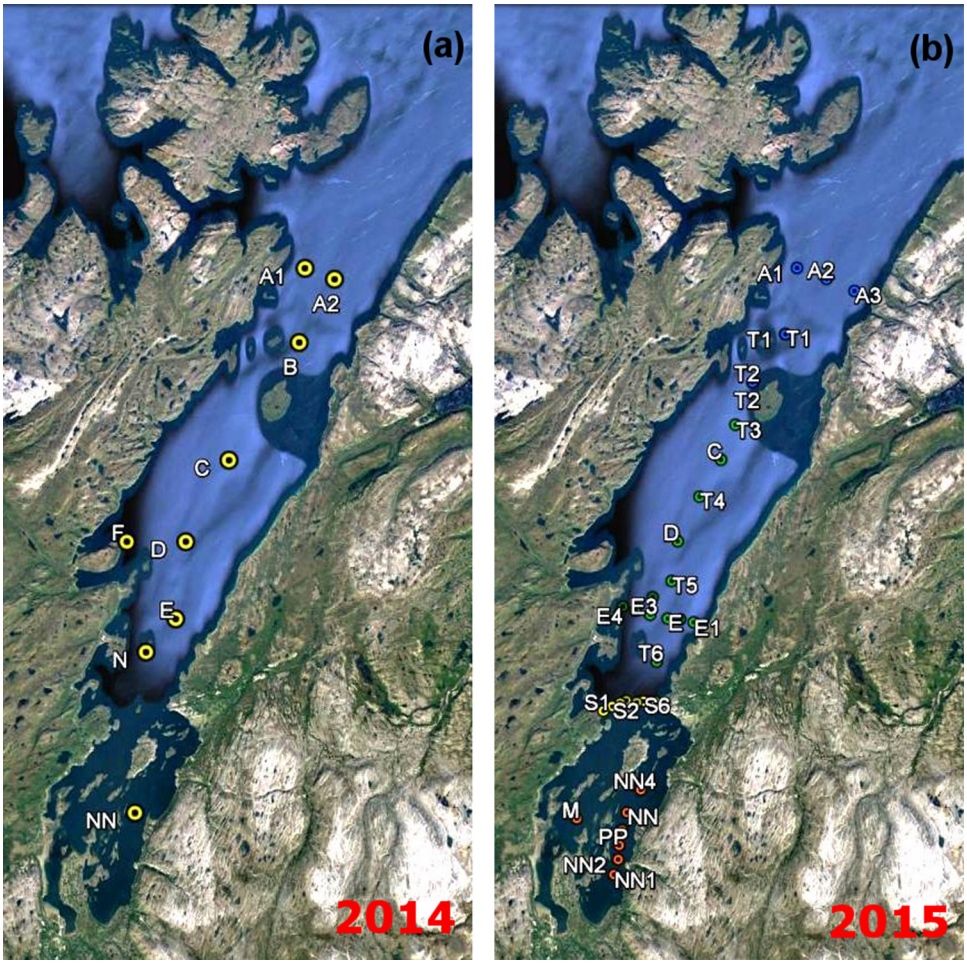

Figure 3 Hydrographic stations visited in (a) 2014 and (b) 2015 (prepared with Google Earth software; Image Landsat, Image IBCAO).

After collection, the water samples were brought to the coastal station laboratory for analysis. The TSM concentration (in g m^{-3}), defined as the dry mass of particles per unit volume of water, was determined using a standard gravimetric technique (Stavn et al., 2009; Woźniak et al., 2011). The water samples were passed through specially prepared GF/F filters (25 mm in diameter). Before filtration, these filters were precombusted for 4 h at 450°C, pre-washed with pure deionized and particle-free water (to prevent the loss of filter material during the filtration of the main sample), dried and pre-weighed. Volumes of seawater samples varied between 250 and 2500 ml, depending on the water turbidity. The samples were filtered as soon as possible after collection. When filtration was completed, the filters were rinsed with about 60 ml purified deionized water to remove sea salt. Next, the filters with their particle load were dried. The dry mass of particles collected on the filters was measured with a Radwag XA 82/220.R2 microbalance (resolution 0.01 mg). Three replicate filters were weighed for each water sample, the reproducibility generally being within ±8%. Thereafter, the filters were combusted for 4 h at 450°C to remove the organic particle fraction (loss on ignition (LOI) technique; Pearlman et al., 1995) and reweighed. The concentration of particulate organic matter (TSM_{org}) was calculated (in g m^{-3}) from the difference in weight before and after combustion. The ac-9 and ac-s data were processed according to procedures described in Pegau et al. (1997). After applying the corrections for water temperature and salinity, the data were carefully inspected for large spikes, most likely present because of the air bubbles in surface waters. For the final data set, data from the upper sections of the profiles were used, which were averaged into 1 m bins in order to average the instrumental noise. Finally, the values from the water sample analysis were matched with simultaneous determinations of beam attenuation coefficient (c_p at 650 nm and 648.8 nm for the ac-9 and ac-s instruments, respectively). These data yielded statistical relationships between the optical and water sample data (Fig. 4). There was a small but systematic difference between the values of $c_p(650)$ recorded by the ac-9 instrument and those of $c_p(648.8)$ recorded by the ac-s. For consistency, therefore, the ac-9 data were converted to the ac-s measurements in accordance with the relationship shown in Fig. 4a. This was done because (1) more data were collected with the ac-s, and (2) the ac-s was new and was calibrated immediately prior to the experiments. Although the correction was relatively small, the vertical profiles measured at the same station with the ac-9 and ac-s were almost identical after it had been applied. In the second step, the relationship based on the comparison between c_p and TSM determined from the water samples shown in Fig. 4b was applied to all the vertical optical profiles of c_p collected *in situ* (converted ac-9 and ac-s data). This

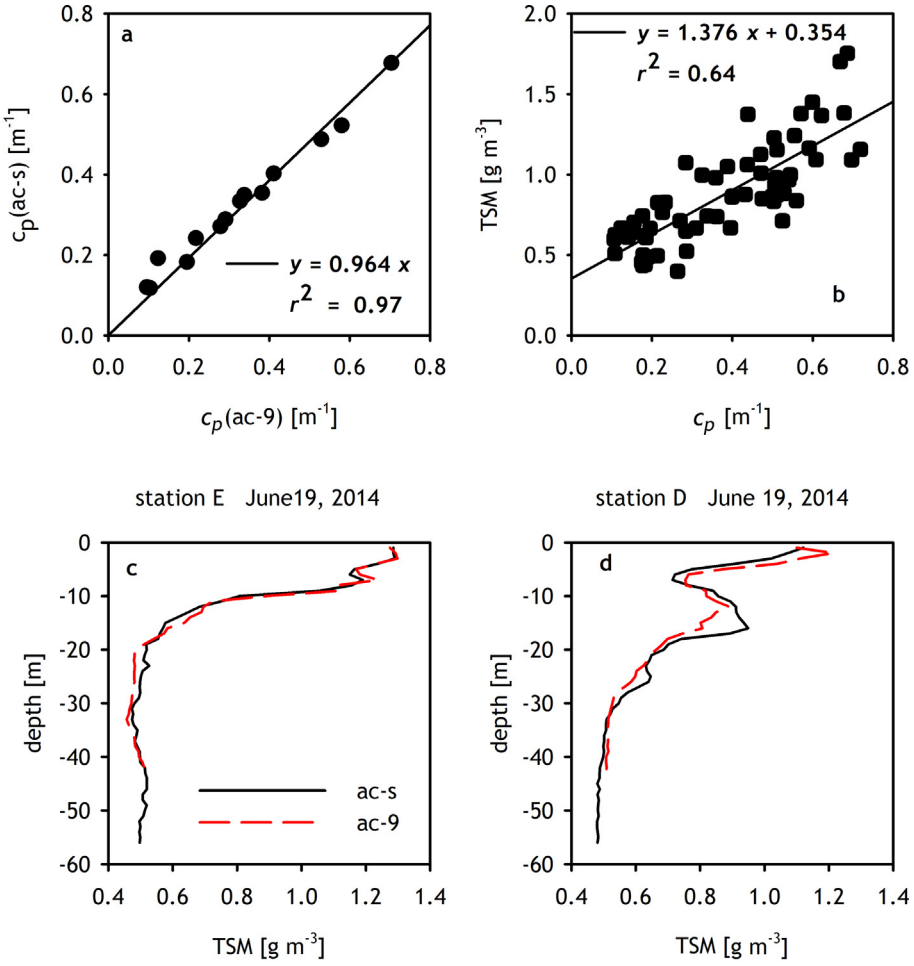

Figure 4 (a) Regression used to convert ac-9 c_p(650) data to c_p(648.8) ac-s values; (b) regression between in water c_p measurements and TSM concentrations determined on water samples; (c) and (d) comparison of example TSM vertical concentration profiles determined from ac-9 and ac-s measurements.

yielded information about the vertical distribution of TSM concentrations. Vertical profiles of TSM derived from ac-9 and ac-s measurements at the same station are exemplified in Fig. 4c and d. The experimental data also contain two samples of water taken from the Rivers Børselva and Lakselva in 2015.

Vertical profiles of water temperature (T) and salinity (S) were collected during the experiment with an SBE 49 FastCAT (Seabird Electronics) CTD Sensor interfaced with the ac-s.

In addition to the boat surveys, surface currents were monitored using the high-frequency (HF) radar system operating in the Porsanger fjord (the radar site's location is shown in Fig. 2a) from June 10 (year day 161) to October 11 (year day 284) in 2014 and from May 28 (year day 148) to August 17 (year day 229) in 2015. More details on the data sets collected are available in a separate paper (Stramska et al., 2016).

In our paper we have also used additional data sets. Wind data from Honningsvåg and Lakselv with hourly resolution, and precipitation data from Honningsvåg, Børselv and Repvåg with daily resolution, were obtained from the Norwegian Meteorological Institute (http://www.yr.no). Fig. 2a shows the geographical positions of Honningsvåg, Lakselv, Børselv and Repvåg. Daily data of water discharge to the fjord based on the E-Hype numerical model (http://hypeweb.smhi.se/europehype/time-series/) from the model subregions indicated in Fig. 2b are also used. That model was extensively validated with observational data (Donnelly et al., 2011, 2015). Water runoff is given as daily averaged water discharge (in $m^3\ s^{-1}$).

4. Results

4.1. Weather conditions

The weather data are summarized in Figs. 5 and 6. Figs. 5a and 6a show time series of wind speed data from the Honningsvåg and Lakselv weather stations in 2014 and 2015 respectively, while Figs. 5b and 6b display the precipitation data from Honningsvåg, Børselv and Repvåg. The bio-optical experiments lasted only few weeks (June 6—29 in 2014 and May 29—June 18 in 2015) but the meteorological data presented in Figs. 5 and 6 start on year day 140 (mid-May) in order to provide background information from the time before the experiments commenced. For example, Fig. 6 shows that around May 24—25, 2015, several days before the experiment started, there was a strong wind

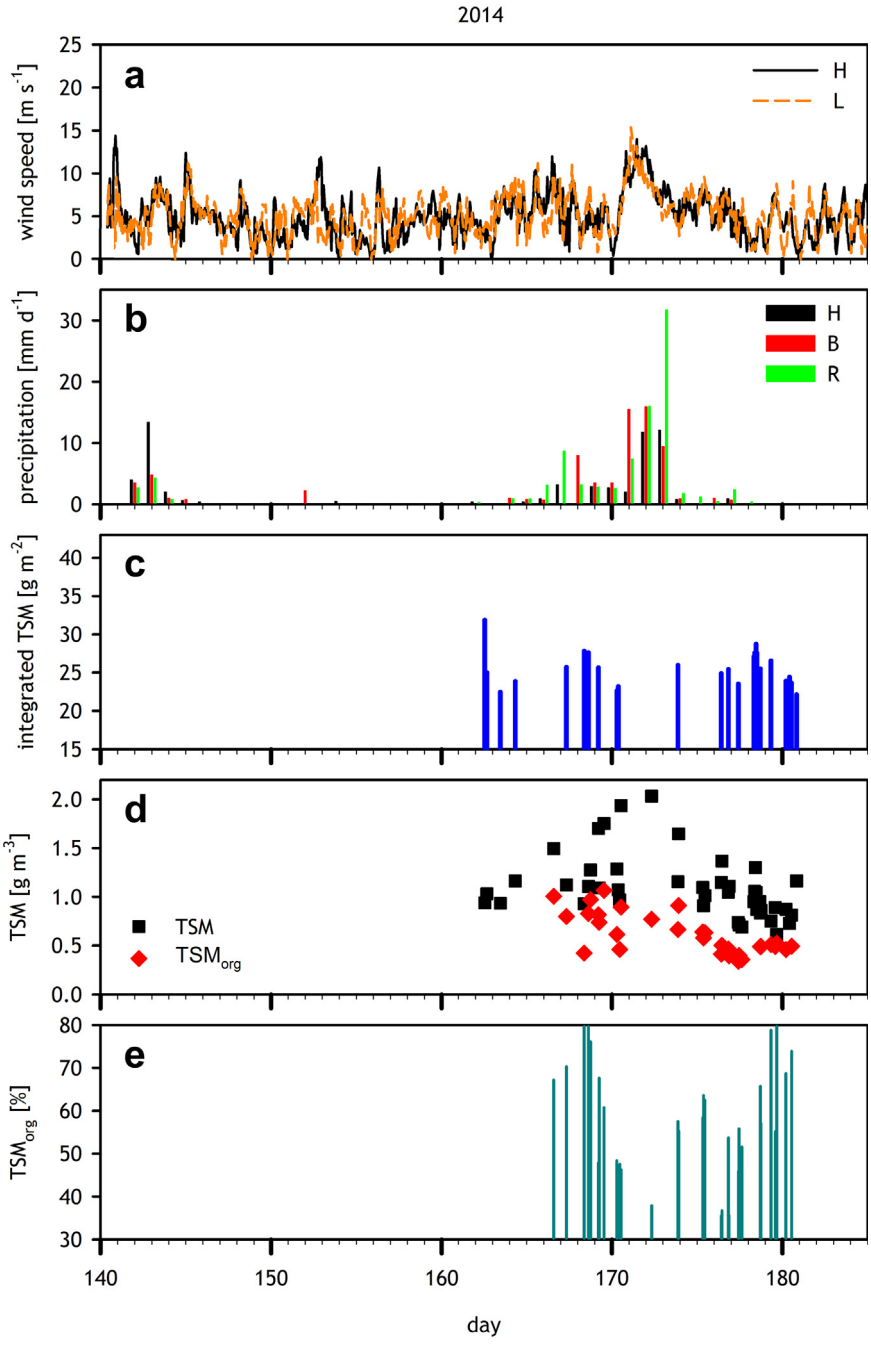

Figure 5 Summary of TSM data collected in 2014. (a) Wind speed recorded at Honningsvåg (H) and Lakselv (L); (b) precipitation at Honningsvåg (H), Børselv (B) and Repvåg (R); (c) TSM integrated over the 0–30 m water layer; (d) concentrations of total TSM and the organic fraction TSM_{org} in surface waters; (e) organic fraction of TSM (in %) in surface waters.

event accompanied by significant precipitation. In May 2014, by contrast, there was much less precipitation and winds were weaker than in May 2015. The lower panels in Figs. 5 and 6 present the results from boat experiments — TSM data from all the stations combined and plotted as a function of time. The water-column-integrated TSM in the top 30 m of the surface water is shown in panels (c), TSM and TSM_{org} concentrations measured in surface waters (0–2 m) are displayed in panels (d), and the percentage of the organic fraction present in surface water TSM is plotted in panels (e). The data shown in panels (c) are based on TSM profiles derived from optical data, the data in panels (d) are a combination of water samples and optical data, while the data in panels (e) refer only to water sample determinations. From Figs. 5 and 6 it becomes clear that the highest TSM values (water-column-integrated and surface concentrations) corresponded to significant precipitation events. These events happened around June 22 (year day 173) in 2014 and around May 25 (day 145) in 2015. Precipitation presumably led to increased water runoff from the coast into the fjord, thereby supplying large amounts of suspended particles to its waters.

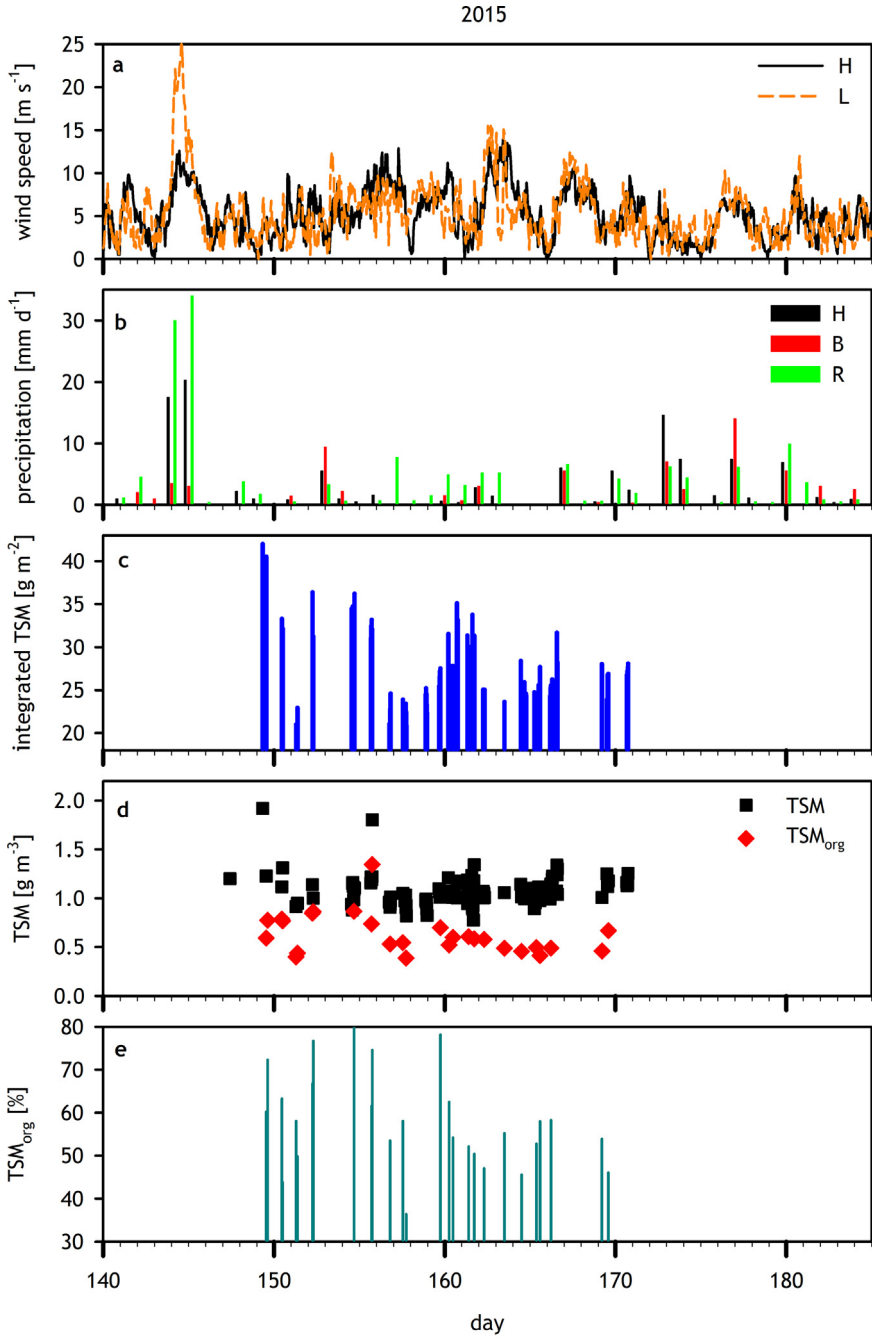

Figure 6 Summary of TSM data collected in 2015. (a) Wind speed recorded at Honningsvåg (H) and Lakselv (L); (b) precipitation at Honningsvåg (H), Børselv (B) and Repvåg (R); (c) TSM integrated over the 0—30 m water layer; (d) concentrations of total TSM and the organic fraction TSM_{org} concentration in surface waters; (e) organic fraction of TSM (in %) in surface waters.

4.2. Terrestrial water discharge

The 2014 and 2015 time series of water discharge in the five subregions of the E-HYPE model for which all runoff is supplied to the Porsanger fjord are shown in Fig. 7 (the locations of the subregions are shown in Fig. 2b). The results from the HYPE model indicate that the average water runoff in this region reaches its annual maximum in June. According to these data, the runoff in subregion 709, where the mouth of the River Lakselva is situated, makes the most important contribution to the total runoff (Fig. 7). Moreover, the temporal distribution of the total discharge was quite different in 2014 and 2015. For better comparison of the data, Fig. 7c shows not only the time series for both years, but also the 36-year averaged values for the period with significant discharge (year days from 100 (April 10) to 200 (July 19)). The total discharge until day 145 was similar in both 2014 and 2015, but the temporal distribution was quite different. For example, on days 120—155 in 2015 the total discharge was about 40% greater than during the same period in 2014. Therefore, the relatively high TSM concentrations measured at the start of the experiment in May 2015

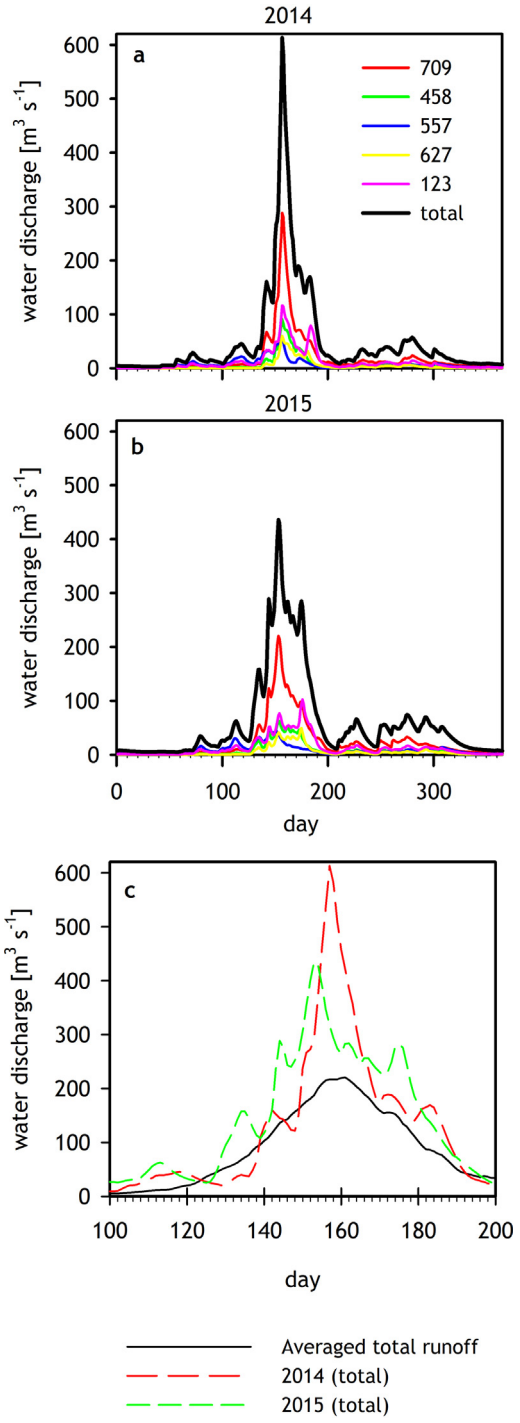

Figure 7 Annual time series of water discharge estimated from the E-Hype model in the subregions marked on the map in Fig. 2, and total runoff estimated as the sum of the water discharge in all the subregions. (a) 2014; (b) 2015; (c) comparison of total runoff in the spring/summer seasons of 2014, 2015, and the 36-year average.

(day 149) were most likely related to both the seasonal runoff of meltwater and the increased runoff due to the precipitation event on days 144–145. In contrast, surface TSM concentrations were lower at the start of the experiment in June 2014 (day 163). According to the data shown in Fig. 7, the total water runoff was also significant at this time, but there were no precipitation events.

At the beginning of the experiment in 2014, the snow near the coast of the fjord had already melted, but some was still melting in the higher mountains in June of that year. The water supplied by the rivers at this time may have contained lower levels of TSM. However, TSM levels inside the fjord increased in 2014 around day 171–173 (June 20–22), most likely due to the storm event with precipitation that occurred around that time. As a result of that event, water was discharged not only by the larger rivers, but also in the form of "no point source water runoff", which could have supplied larger quantities of TSM. The water-column-integrated TSM values were generally higher in 2015 than in 2014, most probably because precipitation was more frequent in 2015. These observations lead to the conclusion that terrestrial water runoff was very likely the most important phenomenon affecting variability of TSM concentrations during this experiment. Table 1 provides detailed statistical information on the TSM concentrations recorded in the Porsanger fjord.

In 2015 data from two rivers (Lakselva and Børselva) were also collected. Measured TSM levels were 11 and 3 g m^{-3} respectively. About 20% of the TSM was organic. Because of insufficient manpower, more regular measurements in the rivers could not be carried out in addition to oceanographic surveys, but the river data do underline the strong variability in TSM concentrations in their waters, and also show that a significant fraction is made up of organic particles (although this fraction was smaller in the rivers than that the average value measured in the fjord waters).

4.3. Water temperature and salinity distribution

There are significant differences between the vertical distribution of water temperature and salinity in subregions 1 and 2, as illustrated in Fig. 8 and in the subsequent figures. The salinity in subregion 1 is quite low at the top of the water column, with values increasing from about 27 at the surface to about 33 at 10 m. It then continues to increase with depth below 20 m, albeit more slowly, to about 34 at depths below 40 m. Since on May 30, 2015, the surface water salinity was the lowest measured by us in this region, it is most likely that large volumes of terrestrial freshwater were also supplied to subregion 1. The surface water temperature (about 8°C) in subregion 1 was generally higher than in subregion 2 (see also Table 2). However, it decreased rapidly with depth to about 4°C or less at 40 m and 2°C at 50 m. The water temperature measured on several occasions in this region at depths below 60 m was only about 0°C (data not shown in Fig. 8 or in Table 2). In contrast, surface (0–2 m) water salinity in subregion 2 varied between 29.13 and almost 33 during this experiment (see Table 2) and depended on the phase of the tide: waters were less saline at low tides (surface water flowing to subregion 2 from subregion 1) but more saline at high tides. The lowest S of 29 was recorded on day 170 in 2014 at station E in the surface waters of subregion 2. Below 40 m in subregion 2 the salinity was always above 34. Also, in contrast to subregion 1, the subsurface water temperature measured during this experiment in subregion 2 (even at 40 m, see Table 2) was always above 4°C. The surface water temperature recorded on May 29 and 30 in subregion 2 was

Table 1 Basic statistics (mean, minimum, maximum, and standard deviation (*SD*) values) of TSM concentrations in three subregions of Porsangerfjorden. *N* stands for number of data taken for the analysis. IN – subregion 1, MID – subregion 2, OUT – subregion 3.

TSM [g m^{-3}]	Mean			Minimum			Maximum			*SD*			*N*		
	IN	MID	OUT	IN	MID	OUT	IN	MID	OUT	IN	MID	OUT	IN	MID	OUT
2014															
0–2 m	1.08	0.96	1.03	0.95	0.72	0.91	1.19	1.32	1.30	0.09	0.20	0.11	6	22	7
40 m	0.58	0.54	0.55	0.55	0.50	0.50	0.64	0.67	0.65	0.04	0.05	0.05	6	22	7
Sum in 30 m	23.99	24.23	27.27	22.14	19.62	24.31	25.85	27.63	31.90	1.46	1.93	2.54	5	19	6
2015															
0–2 m	1.06	1.05	1.10	0.78	0.78	0.88	1.25	1.92	1.31	0.14	0.13	0.12	12	108	14
40 m	0.62	0.63	0.68	0.45	0.47	0.41	0.93	1.08	0.97	0.11	0.08	0.16	12	95	14
Sum in 30 m	24.74	26.48	30.78	17.24	20.92	23.47	28.08	43.15	39.99	3.74	4.28	4.51	12	109	14

Table 2 Basic statistical analysis (mean, minimum, maximum, and standard deviation (*SD*) values) of temperature and salinity in three subregions of Porsangerfjorden. *N* stands for number of data taken for the analysis. IN – subregion 1, MID – subregion 2, OUT – subregion 3.

	Mean			Minimum			Maximum			*SD*			*N*		
	IN	MID	OUT	IN	MID	OUT	IN	MID	OUT	IN	MID	OUT	IN	MID	OUT
Temperature [°C]															
2014															
0–2 m	7.84	7.57	6.75	7.29	6.69	6.62	9.45	8.38	7.06	1.08	0.46	0.15	2	10	4
40 m	4.03	5.27	5.91	2.90	4.15	5.31	5.14	6.09	6.42	1.27	0.54	0.44	2	12	4
2015															
0–2 m	7.55	6.63	6.32	6.22	5.46	5.77	8.18	7.67	7.12	0.48	0.43	0.45	8	103	12
40 m	2.46	4.97	5.67	1.66	4.56	5.04	4.35	5.59	6.18	0.68	0.19	0.39	11	92	12
Salinity															
2014															
0–2 m	29.52	31.35	33.71	26.90	29.13	33.53	30.41	32.81	33.94	1.75	0.68	0.15	2	10	4
40 m	33.85	34.06	34.14	33.69	33.87	34.00	34.02	34.12	34.26	0.19	0.07	0.13	2	12	4
2015															
0–2 m	28.91	31.75	33.79	27.10	25.82	33.37	29.96	33.94	34.15	0.97	1.29	0.20	8	103	12
40 m	33.70	34.12	34.20	33.59	33.95	34.06	33.95	34.23	34.29	0.09	0.05	0.07	11	92	12

lower than that measured in subregion 1. In general (Table 2), the salinity was the highest in subregion 3 owing to significant advection of oceanic water masses. The surface temperature was the highest in subregion 1, whereas the highest temperature at 40 m was noted in subregion 3.

4.4. Temporal and spatial TSM distribution

Since the high TSM concentrations measured at the end of May 2015 produced the most interesting event in this TSM data set, some more data from this period will now be discussed. Fig. 8 presents a few examples of TSM, T and S profiles measured at the end of May 2015. The left-hand side of Fig. 8(plots a–c) presents data from subregion 1, while the right-hand side of Fig. 8(plots d–f) displays data from subregion 2. Unfortunately, it is not possible to state exactly when the TSM concentration reached these elevated levels, because concentrations of about 2 g m^{-3} were already being detected when the first stations has been set up in 2015 (after May 29, Fig. 8). Interestingly, this increase in TSM did not happen at the same time in subregion 1 (see Fig. 8a–c). This is difficult to explain, but it may have been due to larger volumes of runoff water from snow melt being delivered to subregion 2 or because the concentration of suspended matter was higher in the runoff water supplied to subregion 2.

The seasonal increase in TSM concentrations measured along the entire fjord on June 3, 2015 is shown in Fig. 9(a–c). Note that a significant period of time elapsed between the visits to the first station (A2) and the last one (T5) on that day, because of the quite considerable distance (45 km) between them. Station A2 was thus visited as the tide was rising, but T5 was reached at high tide. This implies that some of the variability displayed in Fig. 9 in TSM, T, and S data must be due to spatial patterns and some to the temporal variability associated with tides. Nevertheless, it is clear that elevated TSM concentrations were also recorded in subregion 3 (station A2). In comparison to June 3 (Fig. 9a–c), TSM concentrations on June 10 were somewhat lower (Fig. 9d–f); on that

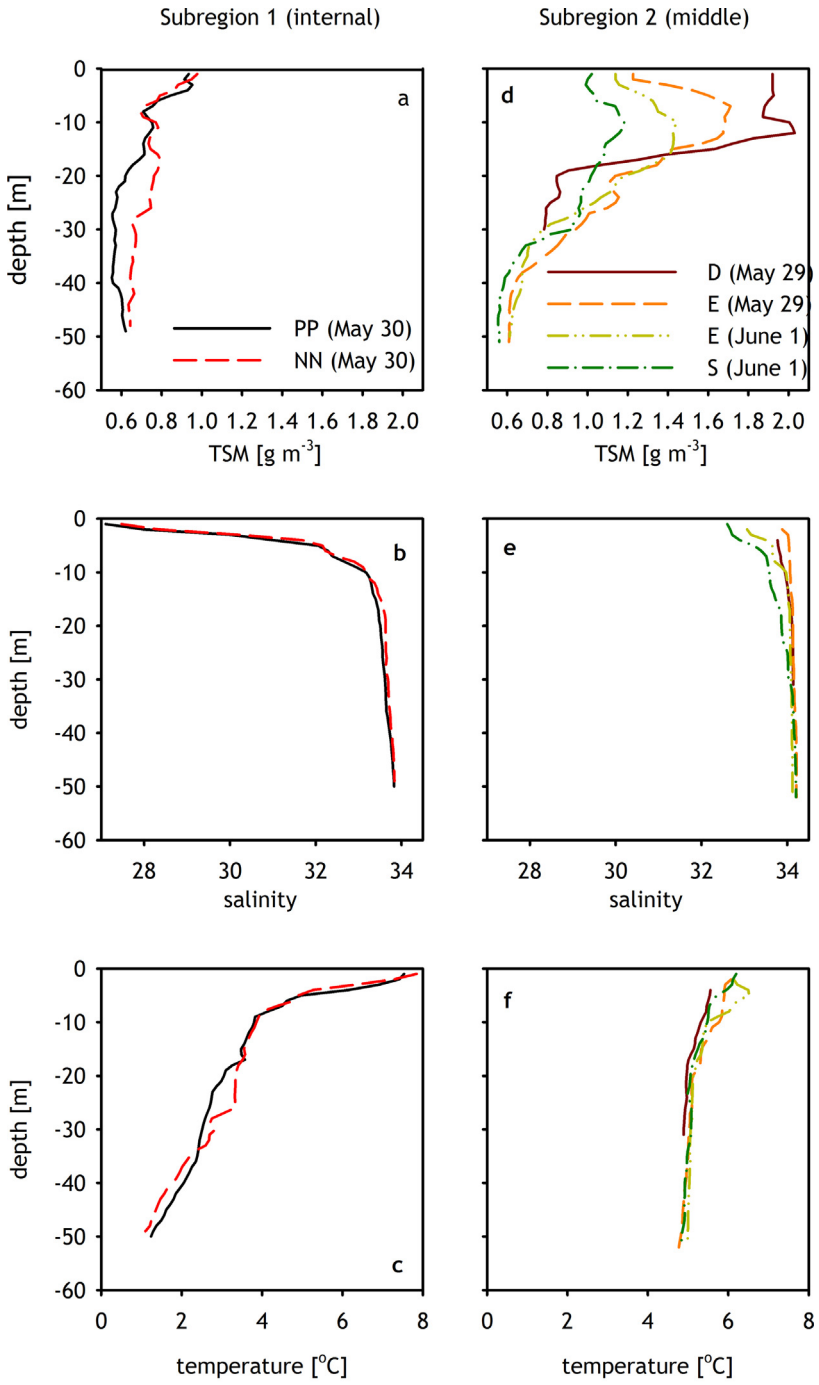

Figure 8 Examples of TSM, water temperature and salinity profiles measured on May 29—June 30, 2015. Note that the range of values for TSM concentration, salinity and temperature is different in each plot.

day, TSM levels were lower in the inner part of the fjord, increasing towards its mouth.

During our experiment it was observed that the spatial variability of TSM documented over a single day was the strongest in the outer part of the fjord (Fig. 10). Fig. 10a shows considerable variability of TSM along transect A in the outer part of the fjord. This was expected, since interaction between oceanic and fjord water masses in subregion 3 is very intensive (see also Table 1). Moreover, the water column in subregion 3 contains at least two water masses with different temperatures—this is also reflected by the TSM concentration profiles. Fig. 11a—f shows examples of data collected across the fjord at similar phases of the tide along transect E in the morning and afternoon of June 9. The vertical TSM profiles at the different stations were quite similar, and the overall pattern did not change much between the morning and afternoon. TSM concentrations were somewhat higher (more than 1.2 g m^{-3}) at about 10 m depth, most likely because water was advected westwards (from station E to station E3). The differences are greater if the same

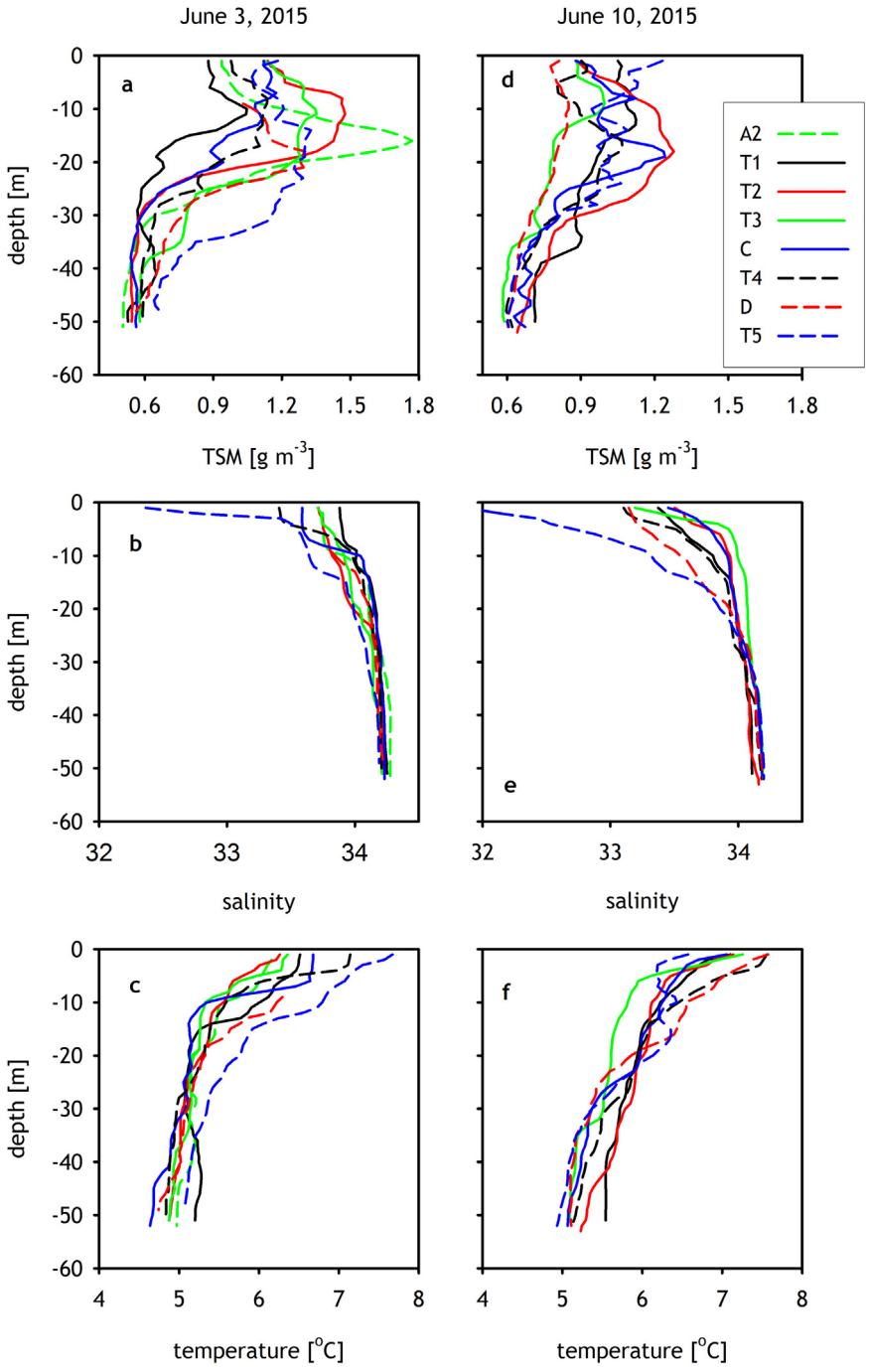

Figure 9 Comparison of example TSM, water temperature and salinity profiles measured at stations located along the fjord (transect T) on June 3 and June 10, 2015.

transect is compared at different phases of the tide (compare Fig. 11a and d with Fig. 11g). The spatial variability of the TSM concentration in the surface waters of subregion 1 appears to be relatively small (Fig. 12).

In general (Table 1), the range of TSM concentrations is the largest in the middle part of the fjord. The mean TSM concentrations at 40 m were 54% and 60% of the surface TSM concentrations recorded in 2014 and 2015 respectively. The mean TSM concentrations were the highest in the inner region in 2014, but in the outer region in 2015. In both years the deep water TSM concentrations were the greatest in subregion 3, which is consistent with the fact that the vertical water density gradient is the smallest in this region and that vertical mixing is expected to play a more significant role in transporting particles to greater depths.

4.5. Suspended organic and inorganic matter

In general, more than half of the suspended matter in the surface waters was organic (on average 55% in 2014 and 59%

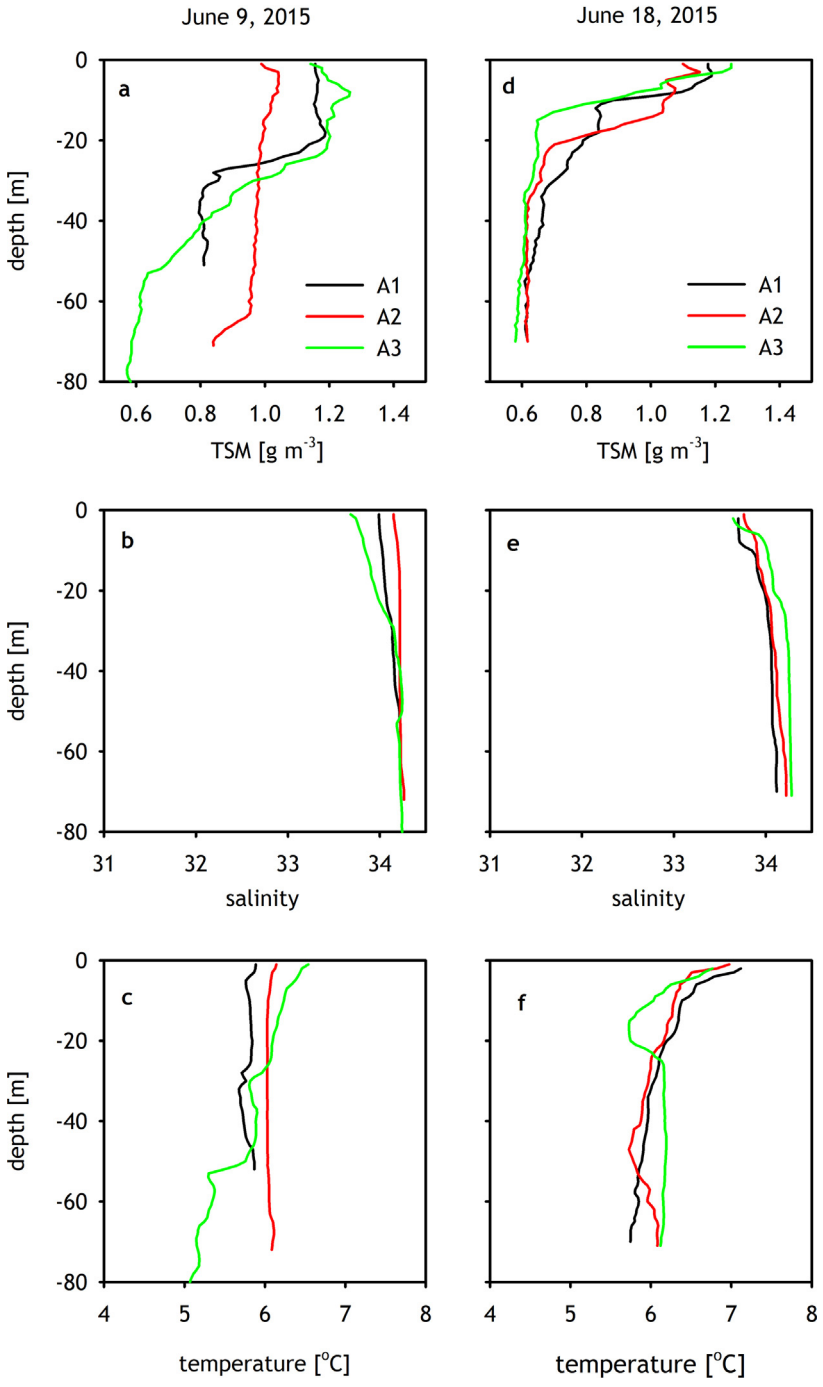

Figure 10 Comparison of example TSM, water temperature and salinity profiles measured at stations located in the outer part the fjord (subregion 3) on June 9 and June 18, 2015.

in 2015). At 40 m and below, this decreased to less than 50% (*e.g.*, June 14 2015, station M) and in some cases even less than 30% (see Figs. 5 and 6). This shows that in the Porsanger fjord, where one would expect relatively low particulate matter concentrations because of the low level of primary productivity and absence of glaciers, TSM concentrations are quite significant and the proportion of mineral particles is relatively high. This is consistent with our observations that rivers supply a large amount of suspended matter, only 20% of which is organic.

5. Discussion

The TSM concentrations measured in the Porsanger fjord (Table 1) are generally high in comparison to other, similar data sets gathered in open ocean regions, but lower than in some fjords, in particular those with glacial runoff. For example, Lund-Hansen et al. (2010) reported TSM concentrations of the order of 300 g m^{-3} in the internal part of the Kangerlussuaq fjord in Greenland. Similar TSM concentrations were measured by Zhu et al. (2016) in Kongsfjorden,

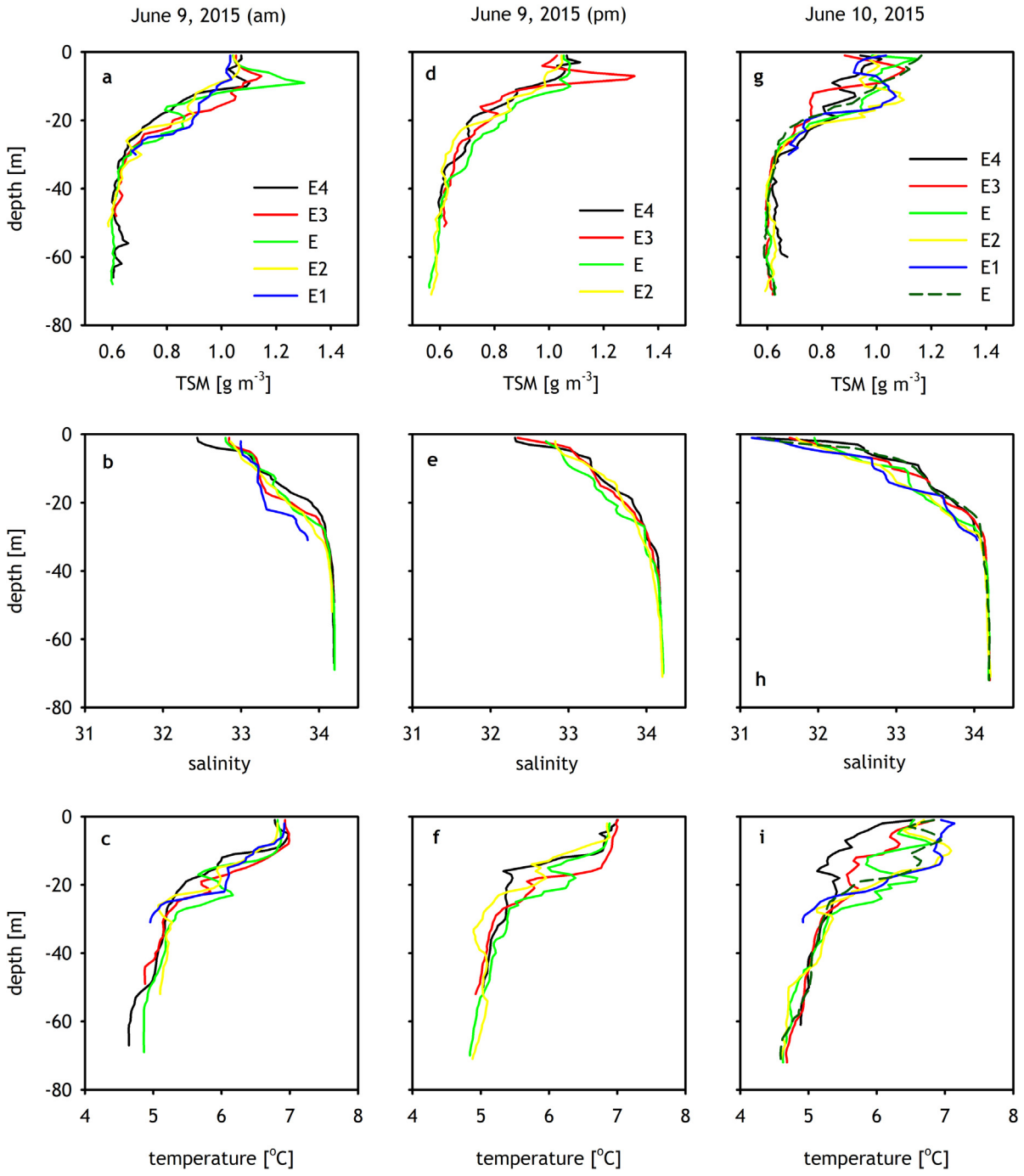

Figure 11 Comparison of example TSM, water temperature and salinity profiles measured at stations located across the middle part of the fjord (subregion 2) on June 9 and June 10, 2015.

Svalbard. In the Baltic Sea (Lund-Hansen and Christianses, 2008; Woźniak et al., 2016) TSM concentrations can also reach high values, for example, more than 15 g m^{-3} in the Gulf of Gdańsk. In the open Baltic Sea TSM concentrations vary between 0.1 and 10 g m^{-3}. The organic fraction in the Baltic Sea is higher (about 80% of TSM there consists of organic particles). The same order of TSM concentrations was recorded in Chesapeake Bay (Ondrusek et al., 2012). In some other coastal regions TSM concentrations are similar to those recorded in this work in the Porsanger fjord (Babin et al., 2003; Faust et al., 2014; Kiyomoto et al., 2001). The mineral content in some coastal regions in the Mediterranean Sea, English Channel or glacial fjords is higher (80, 64, and 81% respectively) than in the Porsanger fjord.

Finally, it has to be noted that our measurements covered only a small part of the year, so no inferences can be drawn regarding the entire annual cycle or the annual range of TSM variability. Nevertheless, considering that this experiment was scheduled for late spring/early summer, when water runoff in the Porsanger fjord is at its most intense, one

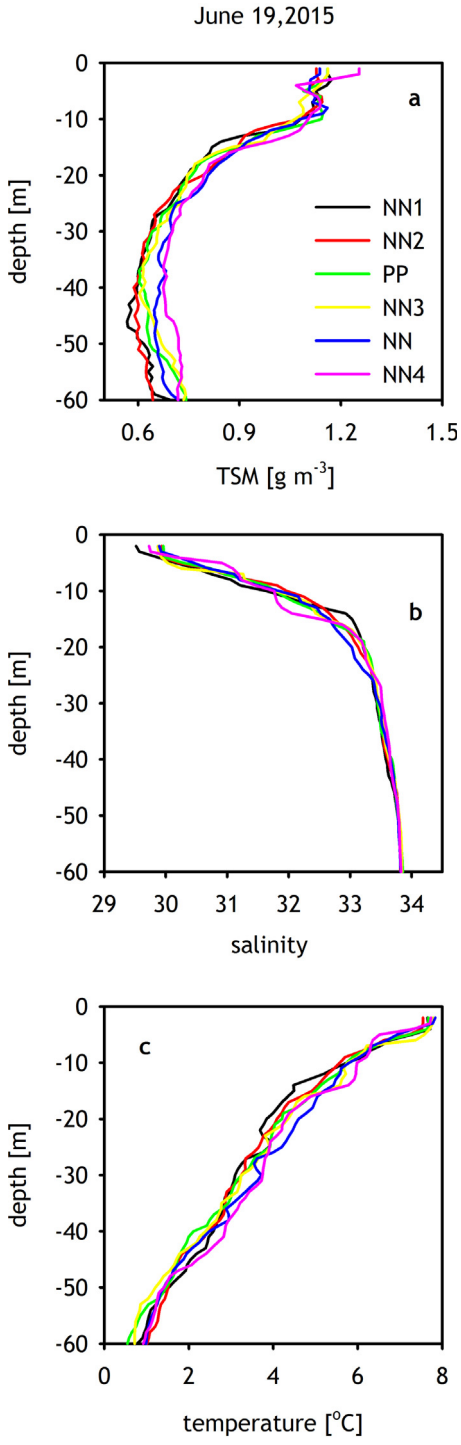

Figure 12 Comparison of example TSM, water temperature and salinity profiles measured at stations located in the inner part the fjord (subregion 1) on June 19, 2015.

can assume that the seasonal increase in TSM concentrations directly related to terrestrial water runoff was reliably documented. One would also expect TSM to increase during summer as a result of seasonal phytoplankton blooms, but this increase would involve mostly the organic fraction of TSM, with the inorganic fraction remaining rather stable. It would be interesting to perform similar experiments in other fjords in order to acquire a better understanding of the range and variability of TSM concentrations in somewhat different environmental settings.

6. Conclusions

On the basis of the *in situ* data presented here, regional bio-optical relationships were derived, enabling optical data (beam attenuation coefficient c_p) to be interpreted in terms of the TSM concentration in the Porsanger fjord. The relationships, similar for the data sets collected in 2014 and 2015, were used to convert *in situ* vertical c_p profiles to TSM concentrations. The results indicate that TSM concentrations lie within the range of values found in other coastal regions, but that they are lower than in fjords where glacial activity supplies large amounts of terrigenous particulate matter. Nevertheless, the present data also indicate that significant amounts of such material are delivered to fjord waters during precipitation events. The optical properties of the fjord waters are most likely affected by this presence of mineral particles, which efficiently scatter underwater light.

A significant temporal variability in TSM concentrations was documented. TSM concentrations in surface waters were the highest during the periods when precipitation events were recorded in the meteorological data. There was also temporal variability in relation to water mass movements associated with tides. Spatial variability was more pronounced when different subregions of the fjord were compared but less so when data from stations located on transects across the fjord were compared. There was a significant decrease in TSM concentration from surface to deep waters. On average, the organic fraction was 56% at the surface and 47% at 40 m depth. The mineral fraction made up some 80% of the TSM delivered to the Porsanger fjord with runoff.

Acknowledgements

The authors express their gratitude to Knut Yngve Børsheim, Hans Kristian Strand, and Henrik Søiland from the Norwegian Institute of Marine Research, for their help with the experiment logistics. Many thanks go to Mateusz Jakowczyk, Daniel Materka, Roman Majchrowski, Roman Marks, Marek Świrgoń and Tomasz Żmójdzin for their participation in the NORDFLUX field experiments. The authors are grateful to all the persons involved in the programmes providing free access to the data sets used in the study. Meteorological data from Honningsvåg were made available by the Norwegian Meteorological Institute (http://www.yr.no). E-Hype model water discharge data were obtained from SMHI (hypeweb.smhi.se). Some of the figures were prepared with Ocean Data View software (Schlitzer, R., Ocean Data View, http://odv.awi.de, 2015), and some maps were prepared using Google Earth software.

This work was funded by the Norway Grants through the Polish-Norwegian Research Programme operated by the National Centre for Research and Development (NCBR contract No. 201985 entitled 'Application of *in situ* observations, high frequency radars, and ocean colour, to study suspended matter, particulate carbon, and dissolved organic carbon fluxes in coastal waters of the Barents Sea'). Partial support for JB and

MS also came from the statutory funds of the Institute of Oceanology of the Polish Academy of Sciences (IO PAN).

References

Babin, M., Morel, A., Fournier-Sicre, V., Fell, F., Stramski, D., 2003. Light scattering properties or marine particles in coastal and open ocean waters as related to the particle mass concentration. Limnol. Oceanogr. 48 (2), 843—859.

Cushman-Roisin, B., Asplin, L., Svendsen, H., 1994. Upwelling in broad fjords. Cont. Shelf Res. 14, 1701—1721.

Donnelly, C., Stromqvist, J., Arheimer, B., 2011. Modelling climate change effects on nutrient discharges from the Baltic Sea catchment: processes and results. IAHS Publ. 348, 145—150.

Donnelly, C., Andersson, J.C.M., Arheimer, B., 2015. Using flow signatures and catchment similarities to evaluate the E-HYPE multi-basin model across Europe. Hydrol. Sci. J. 61 (2), 255—273, http://dx.doi.org/10.1080/02626667.2015.1027710.

Eilertsen, H.C., Frantzen, S., 2007. Phytoplankton from two sub-Arctic fjords in northern Norway 2002—2004: I. Seasonal variations in chlorophyll *a* and bloom dynamics. Mar. Biol. Res. 3, 319—332.

Faust, J.C., Knies, J., Slagstad, T., Vogt, Ch., Milzer, G., Giraudeau, J., 2014. Geochemical composition of Trondheimsfjord surface sediments: sources and spatial variability of marine and terrigenous components. Cont. Shelf Res. 88, 61—71.

Kirk, J.T.O., 2011. Light and Photosynthesis in Aquatic Ecosystems, 3rd ed. Cambridge Univ. Press, 662 pp.

Kiyomoto, Y., Iseki, K., Okamura, K., 2001. Ocean color satellite imagery and shipboard measurements of chlorophyll *a* and suspended particulate matter distribution in the East China Sea. J. Oceanogr. 57, 37—45.

Lund-Hansen, L.C., Christianses, C., 2008. Suspended particulate matter (SPM) in the North Sea-Baltic Sea transition: distributions, inventories, and the autumn 2002 inflows. Danish J. Geogr. 108 (2), 37—47.

Lund-Hansen, L.C., Andersen, T.J., Nielsen, M.H., Pejrup, M., 2010. Suspended matter, Chl-*a*, CDOM, grain sizes, and optical properties in the Arctic Fjord-type Estuary, Kangerlussuaq, West Greenland during summer. Estuar. Coast. 33 (6), 1442—1451.

Mobley, C.D., 1994. Light and Water: Radiative Transfer in Natural Waters. Acad. Press, San Diego, 592 pp.

Montes-Hugo, M., Gagne, J.P., Demers, S., Cizmeli, S., Mas, S., 2012. Ocean colour and distribution of suspended particles in the St. Lawrence Estuary. EARSeL eProc. 11, 1—11.

Ondrusek, M., Stengel, E., Kinkade, C., Vogel, R., Keegstra, P., Hunter, C., Kim, C., 2012. The development of a new optical total suspended matter algorithm for the Chesapeake Bay. Remote Sens. Environ. 119, 243—254, http://dx.doi.org/10.1016/j.rse.2011.12.018.

Pearlman, S.R., Costa, H.S., Jung, R.A., Mckeown, J.J., Pearson, H. E., 1995. Solids (section 2540). In: Eaton, A.D., Clesceri, L.S., Greenberg, A.E. (Eds.), Standard Methods for the Examination of Water and Wastewater. American Publ. Health Assoc, 2-53—2-64.

Pegau, W.S., Gray, D., Zaneveld, J.R., 1997. Absorption and attenuation of visible and near-infrared light in water: dependence on temperature and salinity. Appl. Opt. 36 (24), 6035—6046.

Stavn, R.H., Rick, H.J., Falster, A.V., 2009. Correcting the errors from variable sea salt retention and water of hydration in loss on ignition analysis: implications for studies of estuarine and coastal waters. Estuar. Coast. Shelf Sci. 81 (4), 575—582.

Stramska, M., Jankowski, A., Cieszyńska, A., 2016. Surface currents in the Porsangerfjorden. Pol. Polar Res. 37 (3), 337—360, http://dx.doi.org/10.1515/popore-2016-0018.

Svendsen, H., 1995. Physical oceanography of coupled fjord-coast systems in northern Norway with special focus on dynamics and tides. In: Ecology of Fjords and Coastal Waters. Proc. Mare Nor Symposium on the Ecology of Fjords and Coastal Waters, Tromsø, Norway, 5—9 December 1994, Elsevier, 149—164.

Syvitski, J.P.M., 1989. On the deposition of sediment within glacier-influenced fjords: oceanographic controls. Mar. Geol. 85, 301—329.

Winters, G.V., Syvitski, J.P.M., 1992. Suspended sediment character and distribution in MacBeth Fiord, Baffin Island. Arctic 45, 25—35.

Woźniak, S.B., Meler, J., Lednicka, B., Zdun, A., Stoń-Egiert, J., 2011. Inherent optical properties of suspended particulate matter in the southern Baltic Sea. Oceanologia 53 (3), 691—729, http://dx.doi.org/10.5697/oc.53-3.691.

Woźniak, S.B., Darecki, M., Zabłocka, M., Burska, D., Dera, J., 2016. New simple statistical formulas for estimating surface concentrations of suspended particulate matter (SPM) and particulate organic carbon (POC) from remote-sensing reflectance in the southern Baltic Sea. Oceanologia 58 (3), 161—175, http://dx.doi.org/10.1016/j.oceano.2016.03.002.

Zaneveld, J.R.V., Kitchen, J.C., Moore, C.C., 1994. Scattering error correction of reflecting-tube absorption meters. Proc. SPIE. 2258. Ocean Optics XII 44, http://dx.doi.org/10.1117/12.190095.

Zhu, Z.Y., Wu, Y., Liu, S.M., Wenger, F., Hu, J., Zhang, J., Zhang, R.F., 2016. Organic carbon flux and particulate organic matter composition in Arctic valley glaciers: examples from the Bayelva River and adjacent Kongsfjorden. Biogeosciences 13, 975—987.